Hindawi
Shock and Vibration
Volume 2022, Article ID 3757561, 15 pages
https://doi.org/10.1155/2022/3757561

Research Article

Statistical Estimation of Blast Fragmentation by Applying 3D Laser Scanning to Muck Pile

Qiang Liu,[1] **Fuqiang Shi**,[1] **Xuguang Wang**,[1,2] **and Mingsheng Zhao**[2]

[1]*Southwestern JiaoTong University, Chengdu 430070, China*
[2]*Poly Xinlian Blasting Engineering Group. Co., Ltd, Guiyang 550002, China*

Correspondence should be addressed to Qiang Liu; 631605010132@mails.cqjtu.edu.cn

Received 10 May 2022; Revised 4 July 2022; Accepted 12 August 2022; Published 26 September 2022

Academic Editor: Yonggang Zhang

Run-of-mine fragmentation is an important aspect of mine productivity optimization, as it affects all mine-to-mill processes. The current blasting fragmentation calculation methods do not consider the 3D geometric information. Therefore, their calculation results are imprecise. 3D laser scanning is a technique for extracting the 3D geometric information of an object by constructing a 3D point cloud model, with which extra information on the geometrical characteristics of an object could be captured than with the technique of 2D image processing. In this paper, 3D laser scanning technology was utilized for the calculation of the rock blocks on the surface of a muck pile, and the information about the surface blocks was utilized as the samples for the statistical estimation of blasting fragmentation of muck pile (BFMP). Monte Carlo simulation was utilized as the statistical estimation method for the BFMP. In the lab experiment, results from 2D image processing technique and from 3D laser scanning technique combined with statistical estimate were compared with the physical measurements utilizing a water tank, which show that results with 3D laser scanning are more similar to the physical measurement. Finally, the applicability of 3D laser scanning technology combined with statistical methods to the calculation of blast fragmentation was estimated through field tests in Biesikuduke and Santanghu mine, two open-pit coal mines in Xinjiang Province of western China. Results show that the accuracy of the statistical estimation results of BFMP has a particle size deviation of 1–3 cm.

1. Introduction

Blasting, as an economical and efficient method for breaking rock and ores, has been widely utilized in mining, civil works, and water conservancy and hydropower projects. Blast fragmentation of muck pile (BFMP) is central to the blast results, directly affecting the efficiency of the subsequent loading and transportation process and second delineation of ores [1–3]. Therefore, the research on the calculation method of blasting fragmentation is of great significance.

There are two approaches in vogue to measure the blast fragment size, which are generally divided into direct and indirect categories. Although sieve analysis, which is a direct analysis approach, is the best-suited means with high precision, it is not feasible and practical since the volume of rock blasted is quite large. Common methods of indirect fragmentation prediction analysis include theoretical models, artificial neural network-based approach, two-dimensional (2D) image analysis methods, and three-dimensional (3D) information-based method.

Numerous theoretical models have been developed to predict and measure rock fragmentation. Based on energy loss, Hui and Shuyu [4] deduced the relation equation between explosive unit consumption and fractal dimension of blasting fragmentation distribution. Xiantang and Shihai [5] proposed a theoretical model including damage variables, in which the secondary collision of the blocks affecting the rock fragmentation was considered. However, the geological conditions of mine sites are complicated, and the theoretical model is usually proposed on the basis of many hypotheses, and the influencing parameters are also considered, resulting in the difference between the theoretical model results and the actual situation [6].

Artificial neural network methods have been proposed and developed to cover the above shortages [7–10]. The

factors influencing on blast operation have been fully considered in the methods, including explosive materials, geological conditions, and design of blasting pattern three categories [11–13]. Various factors are selected as input layer parameters, and through multiple blasting cycle sample training, the linear or nonlinear function relationship between these influencing parameters and blasted rock fragments is developed to predict the BFMP [14, 15]. As a disadvantage of this method, too many input factors should be utilized, thereby the engineering practicability would be reduced.

The results of 2D image analysis method show more accurate close to the actual measured value, compared to indirect methods. There are three main commercial software packages which are on the basis of 2D image processing for automatically implementing the calculation of BFMP, including WipFrag, FragScan, and Split-Desktop [16]. The technique of 2D image analysis is a process for the separation of fragments from the surrounding background by means of image segmentation algorithms and then produce the result of BFMP by calculation. In addition, assuming that the block in the image is an equal area circle, the block volume is calculated by the equivalent radius. Realistically, the software packages and techniques of 2D image processing have been utilized in an amount of studies [17, 18] and were reported to overestimate the BFMP by 50–100% of the sieve value [19].

Compared with 2D image analysis, stereophotogrammetry can extract three-dimensional information regarding objects from two or more images (2D) taken at different positions, but extensive manual editing is usually required to delineate overfragments and it is time-consuming [20, 21].

3D laser scanning technology is noncontact measurement technique and can provide more effective and accurate 3D laser point cloud data (3D LPCD) of the muck pile surface blocks with extensive 3D feature information [22], which can enhance the identification of surface blocks and the calculation of the BFMP [23, 24]. In this study, a statistical estimation method combined with 3D laser scanning technology was proposed for the analysis of blasting fragmentation. The information of surface blocks was regarded as the samples, and the 3D laser scanning technology was used to analyze it. At first, amounts of 3D information such as 3D LPCD were collected by means of 3D laser scanning technology and then individually analyzing each block on the surface of the entire blasted muck pile. At last, the data of BFMP was calculated by means of statistical estimation, and the information of individual surface fragments was regarded as the input parameter. By comparing the calculation method proposed in this study with 2D image processing, the results of the new method were more accurate.

2. Apparatus and Software

2.1. Camera and Lens. Images of this study were taken by a camera of SONY ILCE- 6400, a Digital Single Lens Reflex Camera, with approximately 40 million picture elements. In 2D image analysis, small-scale images with 20,010,000 pixels were applied because of the limitation of the software in this research. A standard lens of camera was used, which was a ZEISS BATIS 1.8/85 E LENS with a picture angle of 853–246000.

2.2. 3D Laser Scanner. A FARO 350 laser scanner, which scanning principle is impulse type, was used to create an accurate, complete, and photorealistic 3D image of the muck pile in this study. The specific parameters are as follows: the distance of scanning is 350 m with a reflectivity of 90%, the speed of scanning is 2 million points/second, the accuracy of scanning is 1 mm, the range of scanning is 360° horizontally and 300° vertically, and angular resolution is 19 arcsec.

2.3. Split Desktop. Split Desktop, on a basis of 2D images, is a mainstream software of analyzing fragmentation. Images captured from the object are utilized by Split Desktop and are regarded as a scaling parameter. In this research report, we used a white plastic ball with a diameter of 10 cm as the scaling parameter. Two steps of image delineation were identified after the process of scaling. The first step was automatic delineation, which automatically delineates the image by an image filter. Manual editing was the second step, and the users delineated the image in the automatic delineation step. By calculating the size of the rock block, the size distribution of the rock block was collected as the final output. The following points should be paid attention in the manual editing step, in which one large block could be merged by several small block or broken into several small blocks [16].

3. Statistical Estimation of Blast Fragmentation Based on 3D Laser Point Cloud Data (3D SEBF)

Four headings are demonstrated in this section, which concisely and precisely draw a description of the experimental results, the interpretation, and the experimental conclusions.

The proposed approach could be described by the following steps. First, the 3D LPCD of the blast muck pile is oversegmented into supervoxels by the algorithm of voxel cloud connectivity segmentation (VCCS) [25], and the supervoxels belonging to the same rock block are clustered by the algorithm of locally convex connected patches (LCCP) [26]. Second, the volume of each block is calculated based on its point cloud. The diameter of each individual surface block is calculated by principal component analysis (PCA) [27], and the frequency count is analyzed. Third, based on a frequency count calculation of the diameters of the surface blocks, a probability density function (PDF) and relative cumulative distribution function (CDF), which has a vertical axis of probability density or probability and a horizontal axis of diameter, are determined to fit the size distribution of surface blocks. Finally, the probability was generated randomly by Monte Carlo simulation [28], and its corresponding diameter is calculated utilizing the inverse function of the CDF.

3.1. Rock Block Point Cloud Segmentation and Contour Boundary Recognition. The 3D point cloud of the surface blocks in the muck pile contains sufficient and accurate spatial information of the surface blocks, compared with the 2D rock particle image. Point cloud-based rock block segmentation is classified as a clustering algorithm. For the original point cloud of surface blocks in the muckpile collected by the laser scanner, the octree spatial index (as shown in Figure 1) and the VCCS algorithm are used to form the supervoxel clustering point cloud, among which there are three spatial relations: point adjacency, line adjacency, and surface adjacency. At the beginning of the clustering process, the maximum clustering range R_{seed}, the clustering center R_{voxel}, and the MOV (minimum occupied voxels) should be specified in sequence, as shown in Figure 2. The clustering process is similar to crystallization. Each cluster center starts to calculate the adjacent points at the same time and continuously adds new points with the least difference in characteristics until the result meets the preset conditions, controlled by differential variables

$$D = \sqrt{w_c D_c^2 + \frac{w_s D_s^2}{3R_{\text{seed}}^2} + w_n D_n^2}, \tag{1}$$

where equation (1) is the deviation, D_c, D_n, and D_s are the color deviation, the normal deviation, and the distance deviation, respectively, W is the corresponding weight factor, and R_{seed} is the maximum clustering range.

After a 3D point cloud of the surface rock blocks complete supervoxel clustering, the LCCP algorithm is used to distinguish the convexity concavity of the adjacency between the supervoxels and fuse supervoxels belonging to the same block. The LCCP algorithm uses the extended convex criterion (CC) and sacity criterion (SC) to determine the convexity.

As shown in Figure 3, $\overrightarrow{x_1}$ and $\overrightarrow{x_2}$ represent the central vectors of two adjacent supervoxels, respectively; $\overrightarrow{n_1}$ and $\overrightarrow{n_2}$ represent the normal vectors of two adjacent supervoxels, respectively; $\overrightarrow{d} = \overrightarrow{x_1} - \overrightarrow{x_2}$ is the line vector of $\overrightarrow{x_1}$ and $\overrightarrow{x_2}$. CC criterion uses the angles α_1 and α_2, which between the line vector $\overrightarrow{d}$ and the normal vectors $\overrightarrow{n_1}$ and $\overrightarrow{n_2}$, to judge the convexity concavity of two adjacent supervoxels. When $\alpha_1 < \alpha_2$, as shown in Figure 3(a), the clustering relations of the two adjacent supervoxels are referred to convex abutment. Conversely, it is referred to concave abutment, as shown in Figure 3(b). Because of noise and errors in the point cloud, threshold on α_1-α_2 is set as a filtering to misjudgment on convexity concavity.

CC criterion [29] is described by

$$\text{CC}_b\left(\overrightarrow{p_i}, \overrightarrow{p_j}\right) = \begin{cases} \text{establish } \left(\overrightarrow{n_1} - \overrightarrow{n_2}\right) \cdot \widehat{d} > 0 \vee \left(\beta < \beta_{\text{Thresh}}\right), \\ \text{not establish others,} \end{cases} \tag{2}$$

where $\overrightarrow{p_i}$ and $\overrightarrow{p_j}$ represent two adjacent supervoxels, respectively, $\widehat{d}$ represents the unit vector of $\overrightarrow{d}$; βrepresents the angle between normal vectors $\overrightarrow{n_1}$ and $\overrightarrow{n_2}$, and β_{Thresh} represents the threshold on β.

To remove the misjudgment caused by some small noises, additional criteria must be introduced. If two adjacent supervoxels point clouds are intersected by the same supervoxel point cloud, its concave-convex relation must be the same.

$$\text{CC}_e\left(\overrightarrow{p_i}, \overrightarrow{p_j}\right) = \text{CC}_b\left(\overrightarrow{p_i}, \overrightarrow{p_j}\right) \wedge \text{CC}_b\left(\overrightarrow{p_i}, \overrightarrow{p_c}\right) \wedge \text{CC}_b\left(\overrightarrow{p_j}, \overrightarrow{p_c}\right), \tag{3}$$

where $\overrightarrow{p_c}$ is the common supervoxel point cloud that intersects $\overrightarrow{p_i}$ and $\overrightarrow{p_j}$.

If one of the adjacent surfaces is an independent surface, the CC criterion cannot separate them to be invalid. Hence, the SC criterion needs to be introduced. As shown in Figure 4, $\overrightarrow{s}$ is denoted as the cross product of $\overrightarrow{n_1}$ and $\overrightarrow{n_2}$. SC criteria can distinguish the convexity concavity based on the included angle, which is denoted as ϑ, between $\widehat{d}$and $\overrightarrow{s}$, the larger the included angle is, the more convex the relationship is likely to be formed. In Figure 4, the clustering point clouds in (a) and (b) were recognized as a whole, while those in (c) and (d) were identified as individuals.

SC criterion [29] is expressed as

$$\text{SC}\left(\overrightarrow{p_i}, \overrightarrow{p_j}\right) = \begin{cases} \text{establish } \vartheta\left(\overrightarrow{p_i}, \overrightarrow{p_j}\right) > \vartheta_{\text{Thresh}}\left(\beta\left(\overrightarrow{n_1}, \overrightarrow{n_2}\right)\right), \\ \text{not establish others,} \end{cases} \tag{4}$$

where $\vartheta$is represented as the included angle between the vector connected to the centroid of the two adjacent supervoxel point clouds and the straight line vector intersecting the two adjacent supervoxel point cloud and $\vartheta_{\text{Thresh}}\left(\beta\left(\overrightarrow{n_1}, \overrightarrow{n_2}\right)\right)$ represents the threshold on the include angle between vectors of two adjacent supervoxel point clouds.

In summary, the convex adjacency relation of two adjacent supervoxels point clouds would satisfy the general formula:

$$\text{conv}\left(\overrightarrow{p}_i, \overrightarrow{p}_j\right) = \text{CC}_e\left(\overrightarrow{p}_i, \overrightarrow{p}_j\right) \wedge \text{SC}\left(\overrightarrow{p}_i, \overrightarrow{p}_j\right). \tag{5}$$

The algorithm is used to mark the concave-convex relationship of each small area on the surface of the block point cloud, and the region growing algorithm is used to make the region grow on the convex edge to complete the fusion of the clustering results. The clustering point clouds belonging to the same block are marked with the same label and saved in PCD format. Figure 5 shows the specific fragmentation analysis process.

3.2. Extraction of Rock Particle Size. After the segmentation of the point cloud of the entire muck pile, any single rock block point cloud is extracted for geometric characteristic analysis to obtain the size and volume of the individual rock block.

The principal component analysis (PCA) method is carried out to calculate the longest axis length of the block point cloud, which is the particle diameter. The calculating process is to reduce the 3D LPCD of the block to one

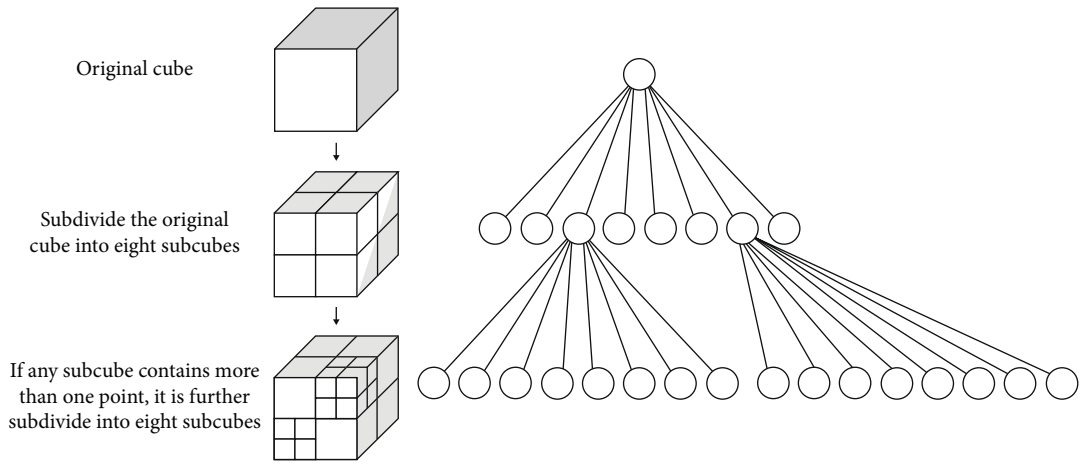

Figure 1: Building an Orthtree in 3D (octree) from a point cloud.

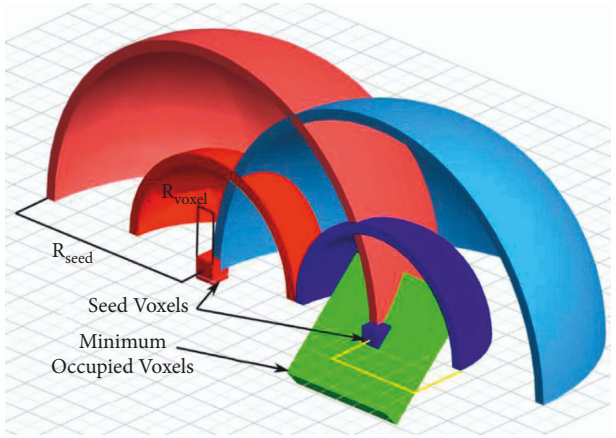

Figure 2: Geometric relations of clustering.

dimension by the PCA method. That is, first, the original point cloud data are composed of n rows and m columns matrix X according to the column; then, zero mean is performed on each dimension of X (namely, the mean value of this column is subtracted); finally, the covariance matrix and its corresponding eigenvalue and eigenvector are solved. The eigenvectors are arranged into a matrix in columns from top to bottom according to the size of the corresponding eigenvalues, and the first k columns are taken to form the matrix P. Reduce the original block point cloud data to the k-dimension by multiplying the matrix P. The difference between the minimum value and the maximum value in the K-dimension data is made, namely, the length of the longest axis of the point cloud of single rock block is obtained.

3.3. Statistical Estimation of Blast Fragmentation Based on Surface Block Size Distribution. The hypotheses of this study are as follows. At first, it is assumed that the blocks are collected from the same location. Thus, the unit weight of each block is the same. On the assumption, the volume ratio can be used to calculate the passing value in the size distribution curve easily [20]:

$$\begin{aligned} \text{passing} &= \frac{m_x}{m_{\text{total}}} \\ &= \frac{\gamma V_x}{\gamma V_{\text{total}}} \\ &= \frac{V_x}{V_{\text{total}}} \times 100\%, m = \gamma V, \end{aligned} \tag{6}$$

where m_x is the cumulative mass, γ is unit weight of rock, and V_x is volume at x.

Second, the shape of each block was regarded as an equivalent circle in hypothesis in 2D image process of Split Desktop software. Therefore, the area of the rock block could be regarded as the area of equivalent circle by calculation:

$$D = \sqrt{\frac{4A}{\pi}}, \tag{7}$$

where D and A are the diameter and area.

The aim of this study is to estimate blasting fragmentation by statistical sampling from the entire muck pile. Firstly, a probability density function (PDF), which matches well with the size distribution of surface rock blocks, was determined by the analysis of frequency count. Secondly, the cumulative distribution function (CDF) was determined from the PDF. The PDF had the vertical axis of probability and the horizontal axis of diameter. The probability was produced at random, and its corresponding diameter was obtained by calculation of the inverse function of CDF. Figure 6 shows the specific statistical analysis process.

For the data comparison between Split Desktop and 3D SEBF, the subsequent performance was carried out. Split Desktop offers area information of each block as the calculation result and used the area information and equation (7) to calculate the equivalent diameter. According to assumption 2, the equivalent diameter was used to calculate the volume of each rock block, and the passing value was obtained by calculation as well. For the volume captured by 3D SEBF, the passing was calculated by equation (6), and the volume was calculated based on the 3D point cloud of each rock block.

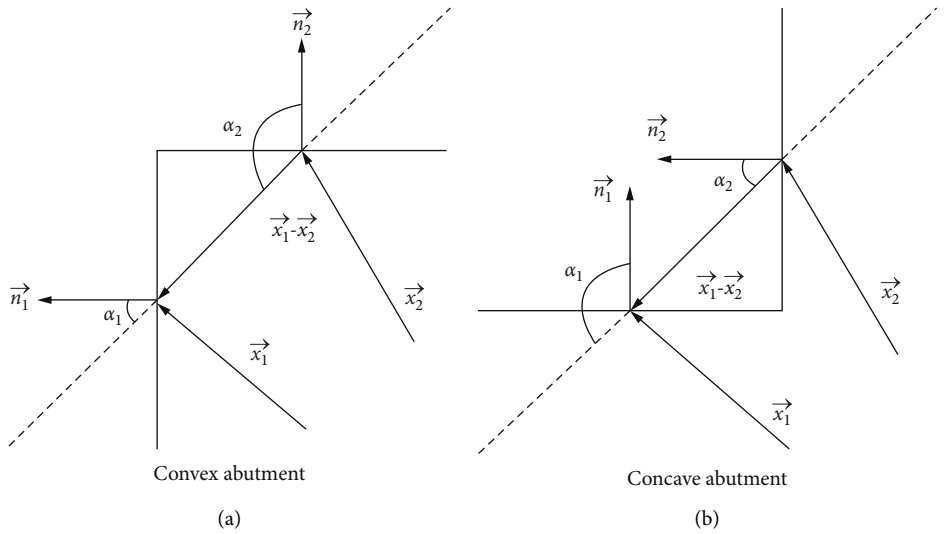

Figure 3: Convex abutment and concave abutment. (a) Convex abutment. (b) Concave abutment.

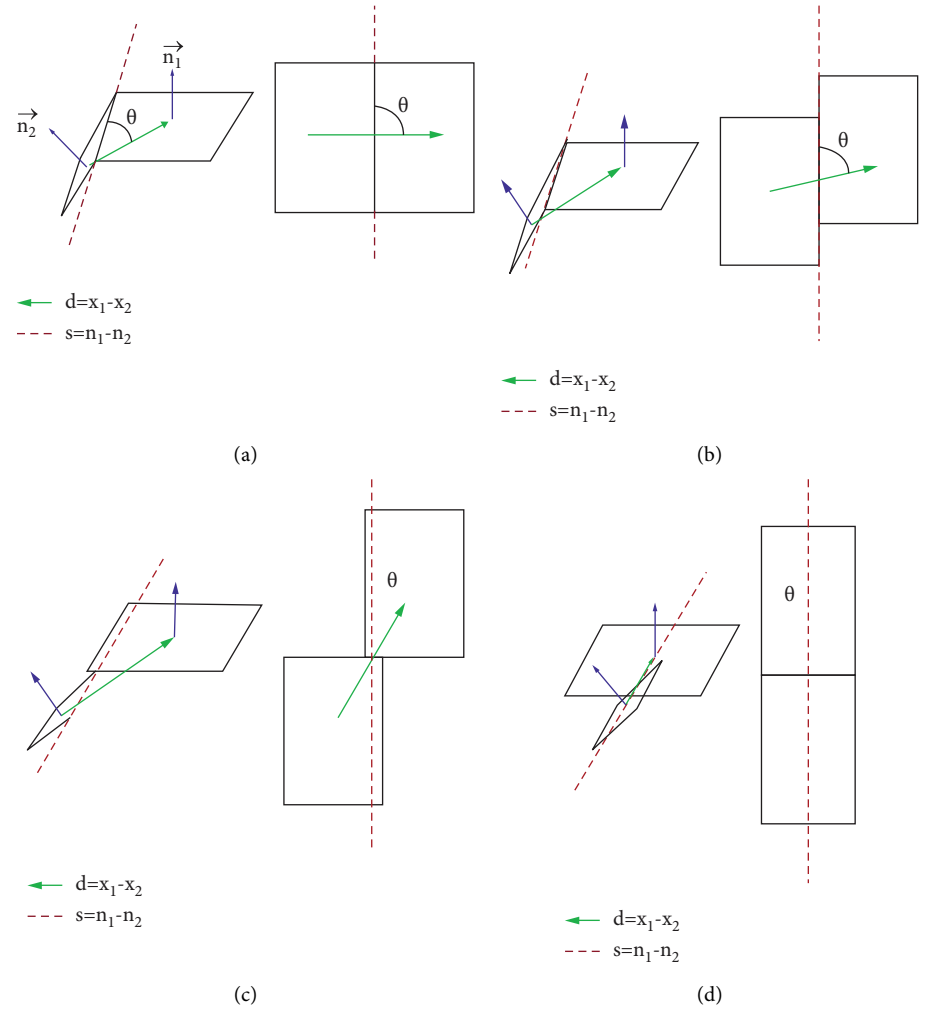

Figure 4: Sanity criterion.

3.4. Modification of Diameter of Rock Blocks. The geometric shape of the intuitively visible part of the surface block can be obtained by 3D laser scanning; however, that of the blocks inside the muck pile cannot be obtained (as shown in Figure 7). Therefore, there is a certain error in the block particle size extracted from the individual block point cloud

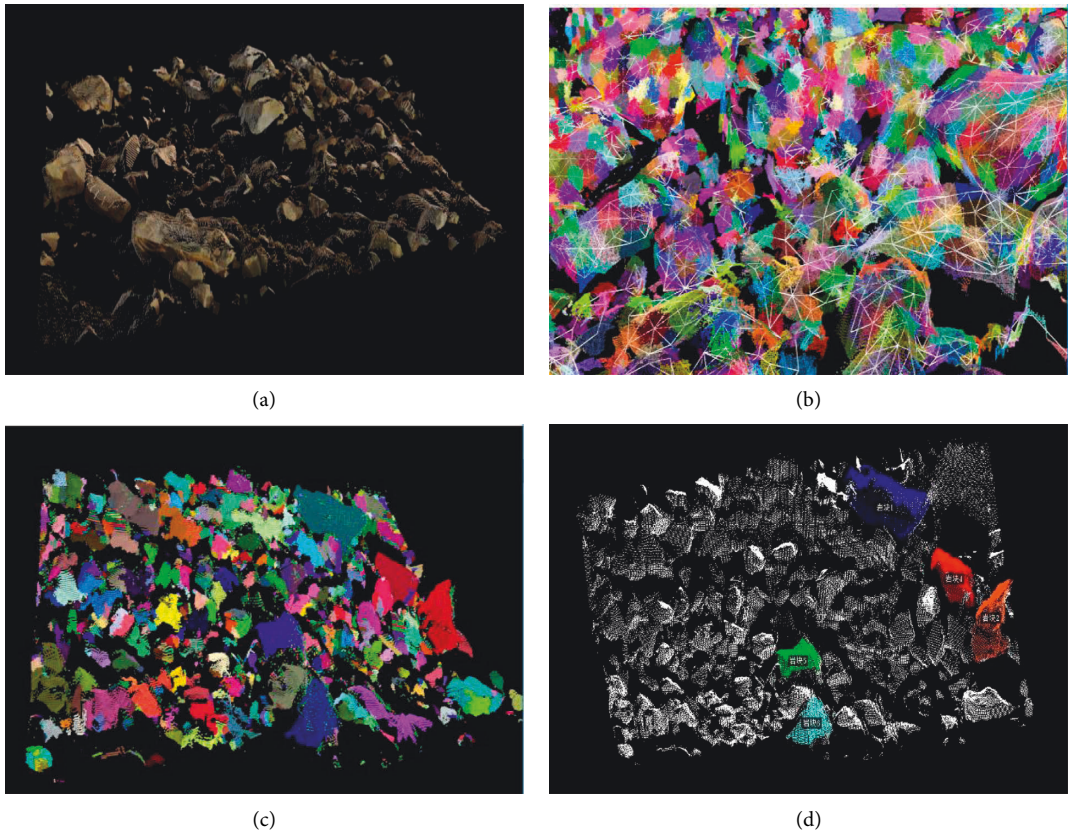

Figure 5: Fragmentation analysis based on the 3D laser scanning technique: (a) point cloud of blast muck pile; (b) supervoxel calculation; (c) block point cloud segmentation; (d) contour extraction for block point cloud.

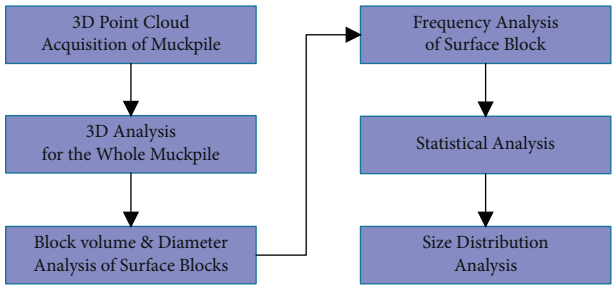

Figure 6: Flowchart of fragmentation analysis based on 3D laser scanning technology (3D SEBF).

separated from the surface block point cloud. The particle size error was estimated by the laboratory and field test. The average particle size measured in the laboratory test was 13.24 cm, while the average particle sizes of the same block pile with two different layouts obtained by the point cloud on the surface blocks were 12.03 cm and 11.87 cm, respectively. The average particle sizes of the two groups of muck pile measured in the field test are 36.29 cm and 37.21 cm, respectively, while the average particle sizes of the same muck pile obtained from the corresponding point cloud were 32.64 cm and 32.98 cm, respectively. The average error ratio of the indoor and outdoor tests was 10.22%, as shown in Table 1. Therefore, at the beginning of the statistical analysis, the method of blast size distribution based on the 3D laser point cloud proposed in this paper requires an increase of 11% to the initially surface block point cloud particle size value before statistical analysis.

4. Application and Discussion

A certain number of rock blocks with different shapes and sizes were selected for the laboratory experiments, which were placed into tilling (as shown in Figure 8) and stacking layouts (as shown in Figure 9), respectively. Results of laboratory experiments from 3D SEBF calculation were compared with those from Split Desktop calculation. In the field tests, the BFMP was calculated using 3D laser scanning.

4.1. Lab Experiments. Thirty-two rock blocks of various shapes and sizes were selected, a vernier caliper was used to measure their diameters and a water tank was used to measure their volumes. The diameter ranged from 4 to 26 cm and the volume ranged from 33 to 9198 cm^3.

4.1.1. Scattered Blocks. In Figure 8, the rock blocks were tiled with two different layouts. Their 2D images were calculated using Split Desktop, and their 3D LPCD was calculated using 3D SEBF, in which results were compared with the results from the constant volume method utilizing a water tank.

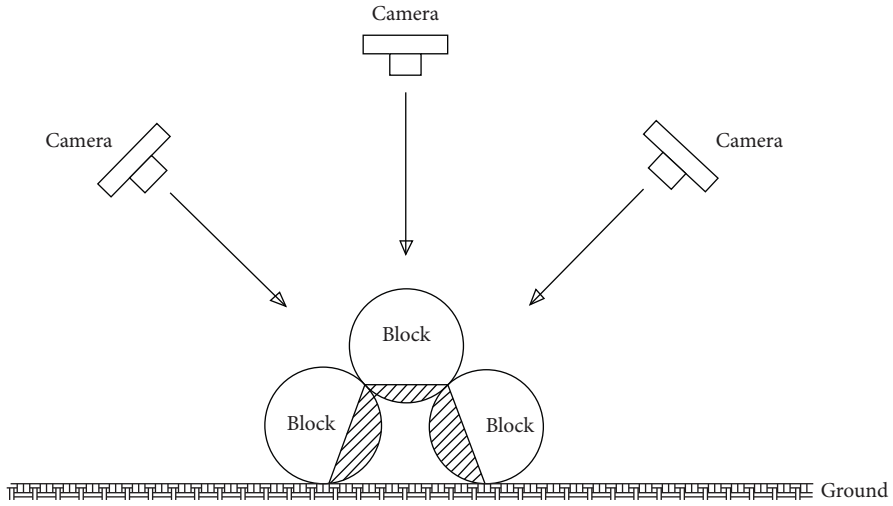

Figure 7: Possible sources of error of stacked blocks.

Table 1: Error of surface rock blocks in stacked blocks.

	Lab experiment			Field test				
		Surface		Test 1		Test 2		
	Entire	Case1	Case2	Entire	Surface	Entire	Surface	
Mean diameter (cm)	13.24	12.03	11.87	36.29	32.64	37.21	32.98	Mean error ratio (%)
Error ratio (%)		9.13	10.34		10.06		11.36	10.22

Figure 10 depicts the size distribution curves of three different calculation methods. From Figure 10, it could be shown that the results of laser-scanner and desk-split were analyzed by the 3D SEBF calculation and Split Desktop calculation, respectively, and the result of water tank was concluded by the constant volume method. Comparing with the measurement of water tank, the degree of accuracy of 3D SEBF calculation results was much higher, while as the diameter became larger, the Split Desktop calculation tended to show greater differences from the water tank measurements, as shown in Figure 10. From the results of Case 1, comparing the 3D SEBF calculation with the measurement of water tank, the maximum deviation of diameter was 0.7 cm, and the mean deviation was 0.18 cm. Meanwhile, the maximum deviation of diameter was 4.8 cm, and the mean deviation was 2.46 cm between the Split Desktop analysis and the measurement of water tank. From the results of Case 2, comparing the 3D SEBF analysis with the measurement of water tank, the maximum deviation of diameter was 1.1 cm, and the mean deviation was 0.4 cm. Meanwhile, the maximum deviation of diameter was 5.9 cm, and the mean deviation was 1.68 cm between the Split Desktop analysis and the measurement of water tank. Figure 10 showed that if the 3D LPCD of individual rock block was used to recognize its overall shape, the 3D SEBF analysis provides the same standard of results as the tank measurements. Hence, each block was modeled separately and utilized as the raw data in the field tests.

4.1.2. Stacked Blocks. In Figure 9, rock blocks were stacked into heaps with various arrangements. According to the results from the frequency count of the surface rock blocks in the muck pile, the size distributions of the surface rock blocks applied a log-normal distribution in both cases (Table 2), and it is expressed by

$$x = F^{-1}(p|\mu, \sigma), \tag{8}$$

$$\begin{aligned} p &= F(x|\mu, \sigma), \\ &= \frac{1}{2} + \frac{1}{2}\operatorname{erf}\left[\frac{\ln x - \mu}{\sigma\sqrt{2\pi}}\right] \\ &= \frac{1}{\sigma\sqrt{2\pi}}\int_0^x \frac{e^{-(\ln t-\mu)^2/2\sigma^2}}{t}dt, \end{aligned} \tag{9}$$

$$f(x|\mu, \sigma) = \frac{1}{x\sigma\sqrt{2\pi}}e^{-(\ln x-\mu)^2/2\sigma^2},\ x > 0. \tag{10}$$

Case 1

(a)

Case 2

(b)

Figure 8: Scattered blocks with various layouts. (a) Case 1. (b) Case 2.

Case1

(a)

Figure 9: Continued.

Case2

(b)

Figure 9: stacked blocks with different layouts in the lab experiments. (a) Case 1. (b) Case 2.

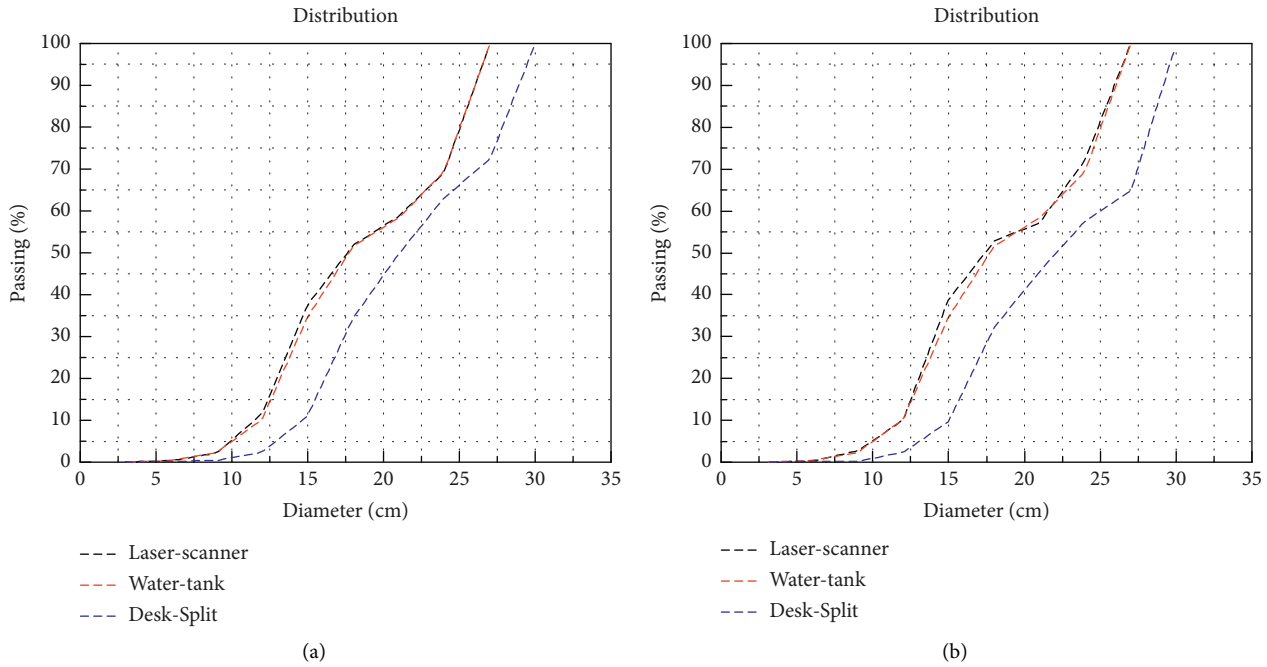

Figure 10: Size distribution of the scattered blocks. (a) Case 1. (b) Case 2.

Table 2: Frequency count for the surface rock blocks in the lab experiments. (a) Case 1. (b) Case 2.

Diameter (cm)	Count	Cumulative count	Relative frequency
(a) Case 1			
(0, 5]	1	1	0.03125
(5, 10]	8	9	0.25
(10, 15]	15	24	0.46875
(15, 20]	5	29	0.15625
(20, 25]	2	31	0.0625
(25, 30]	1	32	0.03125
(b) Case 2			
(0, 5]	3	3	0.09375
(5, 10]	9	12	0.28125
(10, 15]	13	25	0.40625
(15, 20]	5	30	0.15625
(20, 25]	1	31	0.03125
(25, 30]	1	32	0.03125

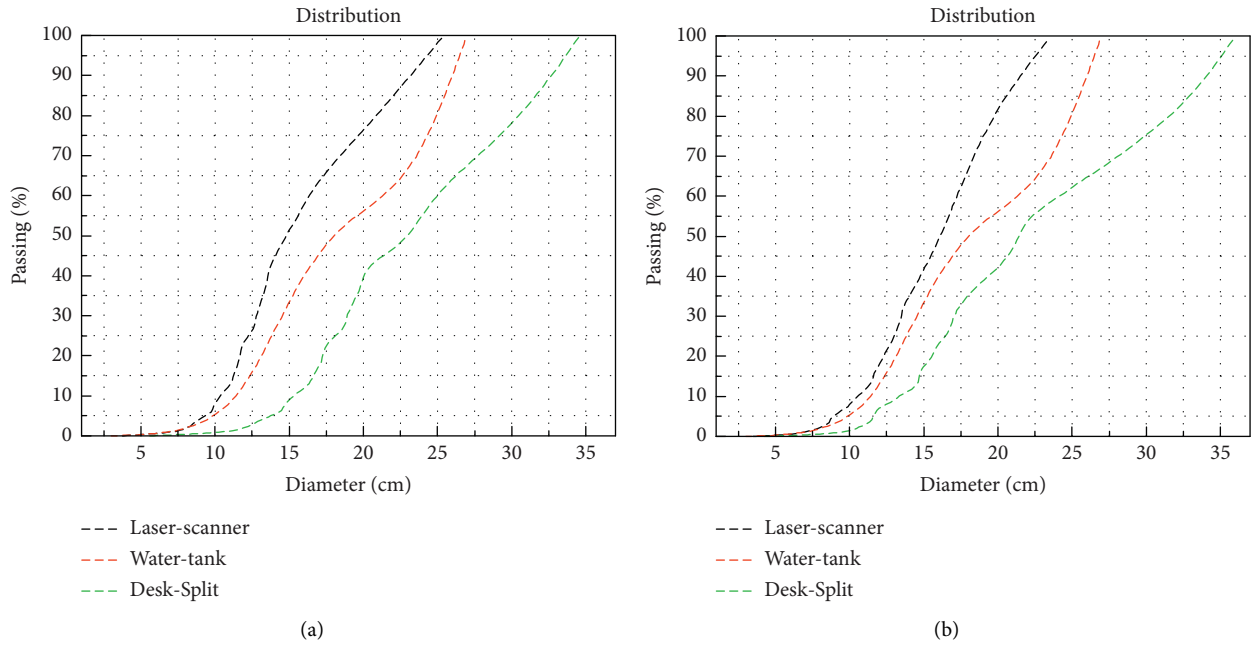

Figure 11: Size distribution of the stacked blocks including the information on the surface blocks. (a) Case 1. (b) Case 2.

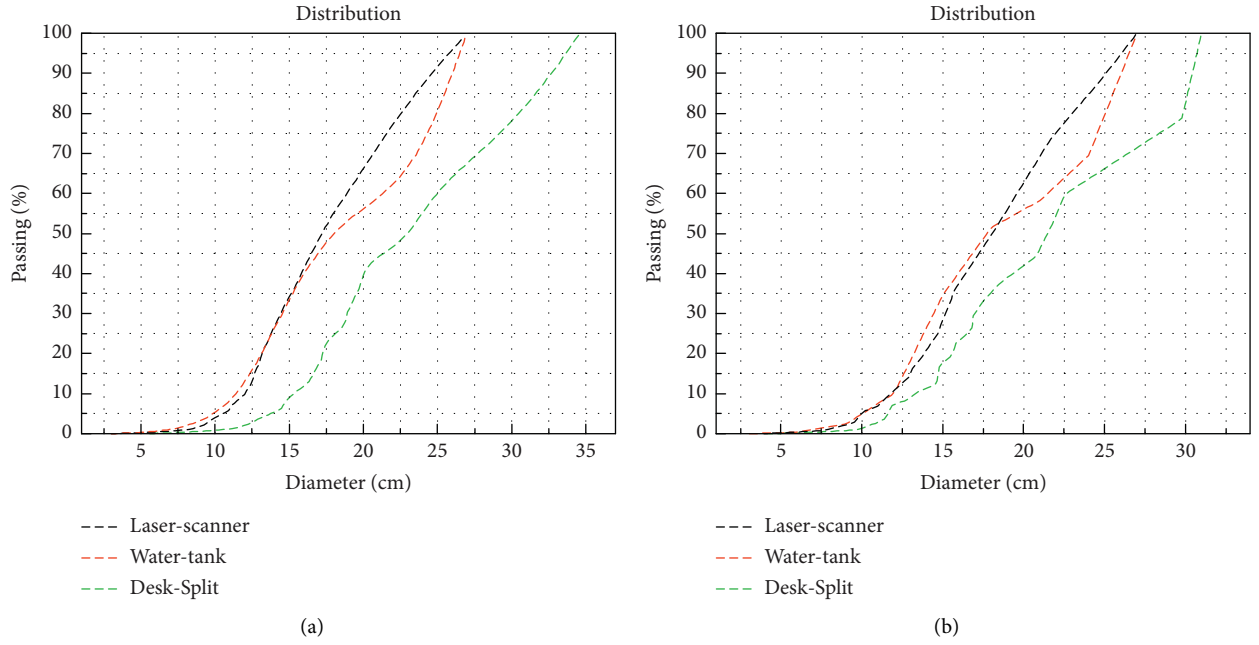

Figure 12: Size distribution of the stacked blocks using interval of the surface blocks and diameter compensation. (a) Case 1. (b) Case 2.

Equation (8) is the inverse function of a log-normal distribution, in which the arguments μ represents the mean deviation and σ represents the standard deviation. Equation (9) is the cumulative distribution function of a log-normal distribution, in which the arguments μ and σ are the input arguments and the natural logarithm of variables. Equation (10) is the probability density function of a log-normal distribution. Thus, in equation (8), μ and σ of the surface blocks were utilized as the input arguments for the statistical estimate of the whole of muck pile. The information about the rock blocks on the surface of a muck piles was extracted with 3D SEBF.

As mentioned in Section 3.3, for a reasonable statistical estimate of blasting fragmentation, the size range of blasting fragmentation has an upper and lower bound:

Test 1 (a) Test 2 (b)

Figure 13: Stacked blocks with different arrangements in the filed experiments. (a) Test 1. (b) Test 2.

Table 3: Frequency count for the surface rock blocks in the field tests. (a) Field 1. (b) Field 2.

Diameter (cm)	Count	Cumulative count	Relative frequency
(a) Field 1			
(0, 15]	5	5	0.04065
(15, 20]	14	19	0.11382
(20, 25]	52	71	0.42276
(25, 30]	21	92	0.17073
(30, 35]	12	104	0.09756
(35, 40]	9	113	0.07317
(40, 45]	7	120	0.05691
(45, 50]	3	123	0.02439
(b) Field 2			
(0, 20]	12	12	0.09677
(20, 25]	24	36	0.19355
(25, 30]	34	70	0.27419
(30, 35]	18	88	0.14516
(35, 40]	16	104	0.12903
(40, 45]	5	109	0.04032
(45, 50]	7	116	0.05645
(50, 55]	4	120	0.03226
(55, 60]	3	123	0.02419
(60, 65]	1	124	0.00806

$$F_T(x) = \int_a^x f_T(t)\mathrm{d}t = \frac{\int_a^x f(t)\mathrm{d}t}{\int_b^x f(t)\mathrm{d}t} = \frac{F(x) - F(a)}{F(b) - F(a)}, \tag{11}$$

$$f_T(x) = \frac{f(x)}{\int_a^b f(x)\mathrm{d}x},\ a \le x \le b, \tag{12}$$

where equation (11) is the interval cumulative distribution function of a log-normal distribution. Equation (12) is the interval probability density function of a log-normal distribution, in which a is the lower and b is the upper bound points.

From the results of Case 1, the maximum and minimum diameters of the rock blocks on the surface were 28.33 cm and 4.12 cm, separately, and the standard and mean deviation of the log-normal distribution of these diameters were 0.21 cm and 2.42 cm, separately. From the results of Case 2, the maximum and minimum diameters of the rock blocks on the surface were 25.62 cm and 3.84 cm, separately, and the standard and mean deviation of the log-normal distribution of these diameters were 0.28 cm and 2.47 cm, separately.

Figures 11 and 12 depict 3D SEBF calculation and Split Desktop calculation were compared with the constant volume method using a water tank. Figure 11 contains the surface rock block information without diameter compensation, and the results in Figure 12 were obtained after truncation and 11% compensation of the surface rock block diameter. Figure 12 shows that calculation with truncation and compensation gives a better performance, with approximate values for maximum and minimum diameters compared to constant volume method using a water tank, while calculation that contains information on surface rock blocks without diameter compensation produced greater deviations in results. In Case 1, the mean deviation between the 3D SEBF calculation and the constant volume method was 1.08 cm, and the maximum deviation was 2.23 cm, while the mean deviation between the Split Desktop calculation and the constant volume method was 4.25 cm, and the maximum deviation was 12.26 cm. In Case 2, the mean deviation between the 3D SEBF calculation and the constant volume method was 1.16 cm, and the maximum deviation was 2.43 cm. The mean deviation between the Split Desktop calculation and the constant volume method was 4.19 cm, and the maximum deviation was 11.26 cm.

Figure 12 also shows that, as the fragment diameter increases, the deviation between results from the Split Desktop analysis and the water tank measurement increases greater.

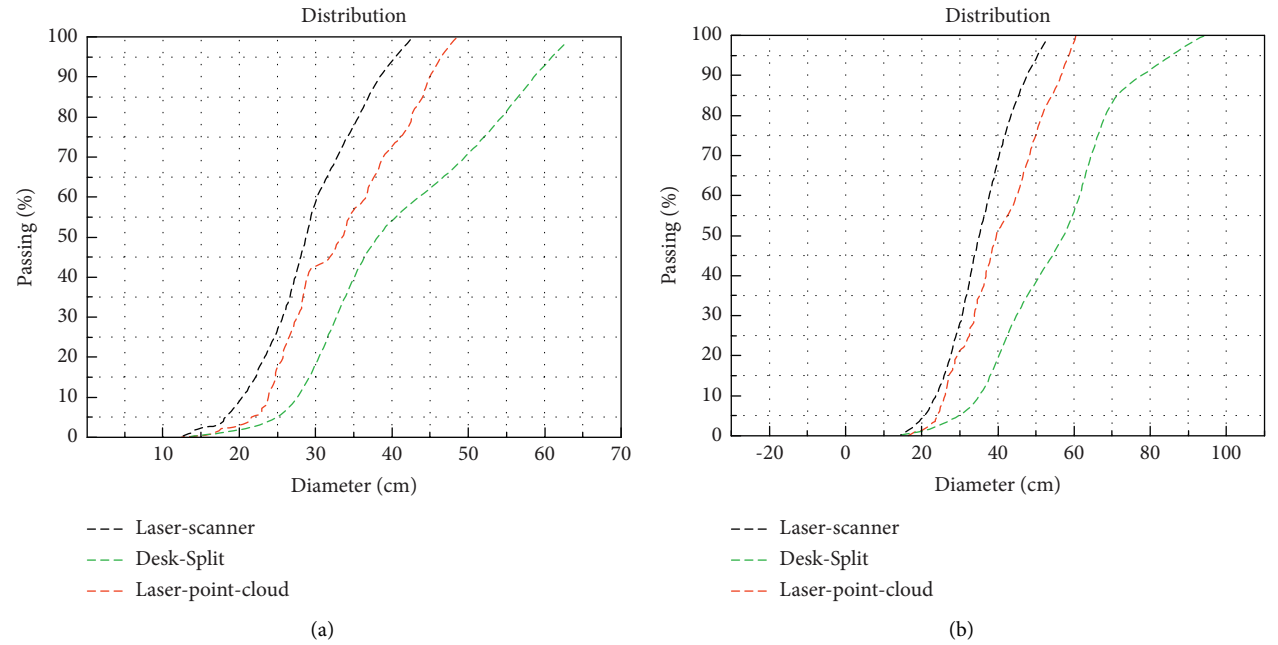

Figure 14: Size distribution of the stacked blocks including the information on the surface rock blocks. (a) Test 1. (b) Test 2.

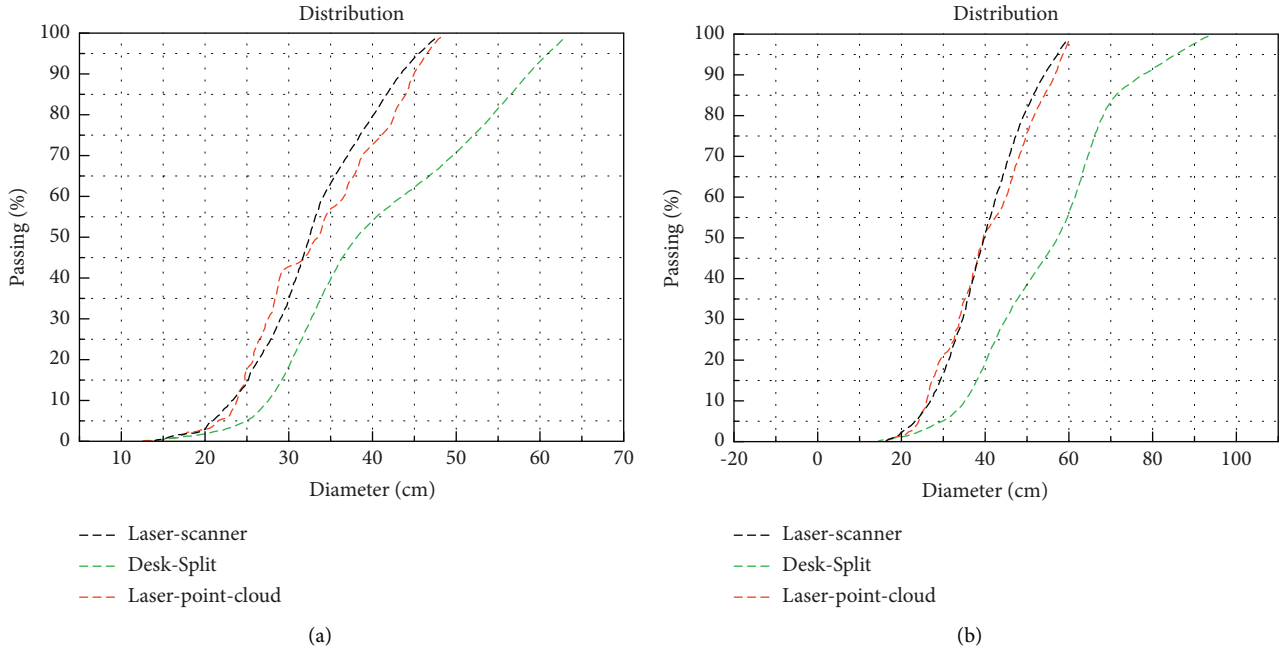

Figure 15: Size distribution of the stacked blocks using diameter compensation and interval of the surface rock blocks. (a) Test 1. (b) Test 2.

4.1.3. Discussion on Lab Experiments. Due to program limitations, Split Desktop uses small size images, while 3D SEBF uses large size 3D point cloud data, which may affect the results. Compared to sieve value, Split Desktop has been reported to underestimate the fine size by approximative 20%, and the average fragment size is likely to be overestimated by about 50% [16]. This research verified that the deviation between the results from Split Desktop analysis and water tank measurement increased with the increase of the fragment diameter. This resulted from the shape of the blocks. For blocks presenting a planar shape, their volume was overestimated due to the equivalent diameter analyzed by Split Desktop, which was utilized to estimate the volume of the planar blocks with assumption 2. 3D SEBF analysis uses the global shape of the blocks by 3D modeling, while Split Desktop uses the area and boundary of the blocks as described previously. Hence, the results of 3D laser scanning are more precise than those of 2D image processing.

4.2. Field Tests. Field tests were conducted in Bescuduke branch plant and Santanghu branch open-pit coal mine of Xinjiang Resources Development Corporation, Xinjiang Province, China. 133 rock blocks were collected from Bescuduke branch plant (site 1), and 135 rock blocks were collected from Santanghu branch plant (site 2), respectively, as shown in Figure 13. As described in Section 4.1.1, the 3D SEBF calculation provides the same standard of results as the tank measurements if each block is modeled separately. Therefore, in the field test, the 3D SEBF calculation method is used to analyze the rock block information. According to 3D SEBF calculation, the volume of site 1 ranges from 1657 to 54062 cm^3, and the diameter ranges from 11.8 to 62.4 cm. Site 2 has a volume range of 2,874 to 89,580 cm^3 and a diameter range of 14.3 to 68.7 cm.

3D SEBF method was used to analyze the surface block information. As shown in Table 3, it was expressed that the size distributions of the surface rock blocks in muck pile in both tests followed log-normal distribution by the frequency count of the surface rock blocks.

In test 1, the calculation of the surface rock block demonstrated that the maximum and minimum diameters were 58.13 cm and 12.24 cm, respectively, and the standard deviation and mean of the log-normal distribution were 0.32 cm and 2.67 cm. In test 2, the calculation of the surface rock block demonstrated that the maximum diameter and minimum diameters was 64.58 cm and 15.37 cm, separately, and the standard deviation and mean of the diameter of the log-normal distribution were 0.28 cm and 3.18 cm. Figure 14 indicates the size distribution curves of muck pile at test 1, and Figure 15 indicates the size distribution curves of muck pile at test 2. Figure 14 contained the surface blocks information, while the results in Figure 15 were obtained by compensating 11% and truncating for the surface blocks diameter. As shown in Figures 14 and 15, estimates using compensation and interval are more precise than those including surface rock blocks information, such as in the lab experiments.

According to the results of the lab experiment, a more precise calculation of blasting fragmentation can be provided by 3D SEBF analysis than the traditional 2D image processing calculation method. The overall experimental results showed that this new approach could be utilized to the calculation of blasting fragmentation, and the error was within 1–3 cm.

5. Conclusion

In this study, the 3D laser scanning technique combined with statistical estimation was utilized to calculate the blasting fragmentation of muck pile, and its applicability was confirmed. The most important considerations are accurate modeling of the samples and a reliable number of samples. In terms of accurate information of samples, 3D laser point cloud information was superior to 2D image processing information. It is significant to obtain enough samples for effective analysis because the more the samples, the more accurate the calculation results. Therefore, this study draws the following conclusions:

(1) The model of muck pile was built and analyzed by the 3D SEBF, and more geometrical characteristics of rock blocks were extracted from the laser point cloud. The result analyzed by this method was more precise compared with 2D image processing.

(2) It was verified, VCCS and LCCP algorithms can be used to distinguish individual block from the entire muck pile based on laser point cloud data, and then PCA analysis can be used to calculate the diameter of surface blocks automatically and accurately.

(3) The accomplishment of the 3D SEBF calculation was promoted by removing rock blocks that had insufficient geometric characteristics and calculating the blocks with a diameter interval of the rock blocks on the surface in the muck pile.

(4) Parts of stacked blocks were concealed because of their layouts in the muck pile. The amount of error introduced by which was evaluated in this study, and the case-dependent approach was used to conduct the statistical estimate after the compensation of the error.

(5) It was verified that the 3D SEBF calculation approach could be used for the calculation of blasting fragmentation. In this study, the mean deviation in diameter ranged from 1 to 3 cm in both the lab experiments and filed tests.

(6) The proposed method makes use of the information of the surface rock blocks in the muck pile. Hence, it is very important to calculate the surface rock blocks with high precision. In block modeling, attention should be paid to ensure that sufficient 3D geometric information is available in block modeling.

Abbreviations

3D: Three-dimensional
2D: Two-dimensional
LPCD: Laser point cloud data
BFMP: Blast fragmentation of muck pile
VCCS: Voxel cloud connectivity segmentation
SDSB: Sizes distribution of surface blocks
LCCP: Locally convex connected patches
PCA: Principal component analysis
3D SEBF: Statistical estimation of blast fragmentation based on 3D laser point cloud data
PDF: Probability density function
CDF: Cumulative distribution function.

Data Availability

All lab and field data in this article used to support the findings of this study are included within the supplementary information file, which is named "Data."

Conflicts of Interest

The authors declare that there are no conflicts of interest regarding the publication of this paper.

Authors' Contributions

Q. L. and F. S. conceptualized the study; Q. L. contributed to methodology and data curation, provided software and resources, and prepared the original draft; Q. L. and X. W. validated the study; F. S. contributed to formal analysis; Q. L. and M. Z. investigated the study; F. S. and X. W. reviewed and edited the manuscript; Q. L. and M. Z. visualized the study; X. W. supervised the study. All authors have read and agreed to the published version of the manuscript.

Acknowledgments

This work was supported by the rock and soil intelligent blasting technology innovation talent team project of Science and Technology Department of Guizhou Province (Guizhou Science and Technology Platform talent (2020), 5019).

Supplementary Materials

This contains lab and field data used in this study. (*Supplementary Materials*)

References

[1] V. M. Kuznetsov, "The mean diameter of the fragments formed by blasting rock," *Soviet Mining Science*, vol. 9, no. 2, pp. 144–148, 1973.

[2] N. Ghaeini, M. Mousakhani, H. B. Amnieh, and A. Jafari, "Prediction of blasting-induced fragmentation in Meydook copper mine using empirical, statistical, and mutual information models," *Arabian Journal of Geosciences*, vol. 10, no. 18, p. 409, 2017.

[3] J. Tao, X. G. Yang, H.-T. Li, J.-W. Zhou, S.-C. Qi, and G.-D. Lu, "Numerical investigation of blast-induced rock fragmentation," *Computers and Geotechnics*, vol. 128, Article ID 103846, 2020.

[4] L. Hui and F. Shuyu, "Theoretical research of the effect on blasting fragmentation distribution from the explosive specific change," *Explosive and Shock*, vol. 17, pp. 359–362, 1997.

[5] Z. Xiantang and C. Shihai, "Study on blast fragmentation for jointed and fractured rock mass considering collision," *Chinese Journal of Rock Mechanics and Engineering*, vol. 21, pp. 1141–1146, 2002.

[6] S. Gheibie, H. Aghababaei, S. H. Hoseinie, and Y. Pourrahimian, "Modified kuz—ram fragmentation model and its use at the sungun copper mine," *International Journal of Rock Mechanics and Mining Sciences*, vol. 46, no. 6, pp. 967–973, 2009.

[7] E. Bakhtavar, H. Khoshrou, and M. Badroddin, "Using dimensional-regression analysis to predict the mean particle size of fragmentation by blasting at the Sungun copper mine," *Arabian Journal of Geosciences*, vol. 8, no. 4, pp. 2111–2120, 2015.

[8] M. Monjezi, H. Amiri, A. Farrokhi, and K. Goshtasbi, "Prediction of rock fragmentation due to blasting in sarcheshmeh copper mine using artificial neural networks," *Geotechnical & Geological Engineering*, vol. 28, no. 4, pp. 423–430, 2010.

[9] E. Ebrahimi, M. Monjezi, M. R. Khalesi, and D. J. Armaghani, "Prediction and optimization of back-break and rock fragmentation using an artificial neural network and a bee colony algorithm," *Bulletin of Engineering Geology and the Environment*, vol. 75, no. 1, pp. 27–36, 2016.

[10] S. Zhang, X.-N. Bui, N.-T. Trung, H. Nguyen, and H.-B. Bui, "Prediction of rock size distribution in mine bench blasting using a novel ant colony optimization-based boosted regression tree technique," *Natural Resources Research*, vol. 29, no. 2, pp. 867–886, 2020.

[11] P. H. S. W. Kulatilake, W. Qiong, T. Hudaverdi, and C. Kuzu, "Mean particle size prediction in rock blast fragmentation using neural networks," *Engineering Geology*, vol. 114, no. 3-4, pp. 298–311, 2010.

[12] C. Xie, H. Nguyen, X.-N. Bui, Y. Choi, J. Zhou, and T. Nguyen-Trang, "Predicting rock size distribution in mine blasting using various novel soft computing models based on meta-heuristics and machine learning algorithms," *Geoscience Frontiers*, vol. 12, no. 3, Article ID 101108, 2021.

[13] I. Enayatollahi, A. Aghajani Bazzazi, and A. Asadi, "Comparison between neural networks and multiple regression analysis to predict rock fragmentation in open-pit mines," *Rock Mechanics and Rock Engineering*, vol. 47, no. 2, pp. 799–807, 2014.

[14] S. Shams, M. Monjezi, V. J. Majd, and D. J. Armaghani, "Application of fuzzy inference system for prediction of rock fragmentation induced by blasting," *Arabian Journal of Geosciences*, vol. 8, no. 12, pp. 10819–10832, 2015.

[15] W. Renjie, L. Haibo, Y. Chong, and X. Xiang, "Model for blasting fragmentation prediction based on statistical classification," *Chinese Journal of Rock Mechanics and Engineering*, vol. 37, pp. 141–147, 2018.

[16] Q. Liu and H. Tran, "Comparing systems — validation of FragScan, WipFrag and split," in *Measurement of Blast Fragmentation,* Routledge, London, UK, 2018.

[17] G. Zhao, B. Dai, C. Ma, L. Zhang, and S. Wang, "Research and application on blasting fragmentation image processing based on 3DFR algorithm," *Journal of Central South University (Science and Technology*, vol. 44, pp. 2002–2007, 2013.

[18] A. I. Lawal, "A new modification to the Kuz-Ram model using the fragment size predicted by image analysis," *International Journal of Rock Mechanics and Mining Sciences*, vol. 138, Article ID 104595, 2021.

[19] J. P. Latham, J. Kemeny, N. Maerz, M. Noy, J. Schleifer, and S. Tose, "A blind comparison between results of four image analysis systems using a photo-library of piles of sieved fragments," *Fragblast*, vol. 7, no. 2, pp. 105–132, 2003.

[20] J.-H. Han and J.-J. Song, "Statistical estimation of blast fragmentation by applying stereophotogrammetry to block piles," *International Journal of Rock Mechanics and Mining Sciences*, vol. 68, pp. 150–158, 2014.

[21] J.-H. Han and J.-J. Song, "Block delineation algorithm for rock fragmentation analysis," *International Journal of Rock Mechanics and Mining Sciences*, vol. 82, pp. 48–60, 2016.

[22] J. Wajs, P. Trybała, J. Górniak-Zimroz, J. Krupa-Kurzynowska, and D. Kasza, "Modern solution for fast and accurate inventorization of open-pit mines by the active remote sensing technique—case study of mikoszów granite mine (lower silesia, SW Poland)," *Energies*, vol. 14, no. 20, p. 6853, 2021.

[23] I. Onederra, M. J. Thurley, and A. Catalan, "Measuring blast fragmentation at Esperanza mine using high-resolution 3D laser scanning," *Mining Technology*, vol. 124, no. 1, pp. 34–36, 2015.

[24] M. J. Thurley, "Automated online measurement of limestone particle size distributions using 3D range data," *Journal of Process Control*, vol. 21, no. 2, pp. 254–262, 2011.

[25] J. Papon, A. Abramov, M. Schoeler, and F. Worgotter, "Voxel cloud connectivity segmentation - supervoxels for point clouds," in *Proceedings of the Computer Vision & Pattern Recognition*, OR, USA, June 2013.

[26] S. C. Stein, F. Wrgtter, M. Schoeler, J. Papon, and T. Kulvicius, "Convexity based object partitioning for robot applications," in *Proceedings of the IEEE International Conference on Robotics & Automation*, Hong Kong, China, June 2014.

[27] A. L. M. Levada, "PCA-KL: a parametric dimensionality reduction approach for unsupervised metric learning," *Advances in Data Analysis and Classification*, vol. 15, no. 4, pp. 829–868, 2021.

[28] M. A. Morin and F. Ficarazzo, "Monte Carlo simulation as a tool to predict blasting fragmentation based on the Kuz–Ram model," *Computers & Geosciences*, vol. 32, no. 3, pp. 352–359, 2006.

[29] S. C. Stein, M. Schoeler, J. Papon, and F. W. Bernstein, "Object partitioning using local convexity," in *Proceedings of the Computer Vision & Pattern Recognition*, OH, USA, June 2014.